Gravity and uplift rates observed in southeast Alaska and their comparison with GIA model predictions

Tadahiro Sato,[1] Satoshi Miura,[1] Wenke Sun,[2] Takayuki Sugano,[3] Jeffrey T. Freymueller,[4] Christopher F. Larsen,[4] Yusaku Ohta,[1] Hiromi Fujimoto,[1] Daisuke Inazu,[1] and Roman J. Motyka[4]

[1]   Over 3 years from 2006 to 2008 we conducted absolute gravity (AG) measurements at 6 sites in and around Glacier Bay (GB) in Southeast Alaska (SE-AK). At two of the 6 sites, AG measurements had been carried out in 1987 by a group from IGPP at UCSD. Mean gravity change rates (unit: μGal/yr, 1 μGal = 10^{-8} ms^{-2}) over the 6 sites are estimated to be -4.50 ± 0.76 and -4.30 ± 0.92 by only using our data and also using the 1987 data, respectively. We computed the uplift and gravity rates predicted by ice load models for three different time intervals: Last Glacial Maximum (LGM), Little Ice Age (LIA) and Present-Day (PD). Except for 1–2 examples, the predictions recover the observed rates within the observation errors. We also estimated the viscous portion of the ratio (unit: μGal/mm) of the observed gravity rate to the uplift rate by correcting for the effects of the Present-Day Ice Mass Change (PDIMC). Two PDIMC models are compared, which are called here as UAF05 and UAF07. Mean ratios are estimated to be -0.205 ± 0.089 and -0.183 ± 0.052 for the cases using UAF05 and UAF07, respectively. The predicted mean ratios are -0.166 ± 0.001 and -0.171 ± 0.002 for the cases using both the LGA and LIA ice models and only using the LIA ice model, respectively. We have confirmed that our AG and GPS observations detect the rates and ratios reflecting an early stage of viscoelastic relaxation mainly due to the unloading effects after the LIA.

1. Introduction

[2]   Since the 1990s, the geodesy and glaciology groups of the University of Alaska, Fairbanks (UAF) have developed a GPS network in Southeast Alaska (SE-AK) and the neighboring region of Canada (Figure 1). One of the purposes of the GPS network is to study GIA (Glacial Isostatic Adjustment) processes in SE-AK. The vertical velocity distribution obtained from the network indicates that SE-AK shows rapid uplift rates up to 35 mm/yr, which are considered to be closely related to the wastage of the glaciers and icefields since the end of the LIA, including the effects of PDIMC [*Larsen et al.*, 2004, hereinafter referred to as GJI2004; *Larsen et al.*, 2005, hereinafter referred to as EPSL2005]. The main results of GJI2004 and EPSL2005, which were derived from the comparisons between the observed uplift rates and the model predictions and the study for the distribution of χ^2 of the residuals (i.e., the differences of the observation to the model prediction) in the 2-parameter space of the lithospheric thickness and the asthenospheric viscosity, are; (1) the effects of unloading since the end of the LIA are the dominant contribution to the observed uplift rates, (2) there must be a low viscosity asthenosphere on the order of 3.7×10^{18} Pa s to 1.4×10^{19} Pa s beneath SE-AK and (3) the lithospheric thickness must be of 60–70 km. *Sato et al.* [2011] discussed the viscoelastic and elastic responses to the past and present-day ice changes based on 91 GPS velocity data, which combined the data previously published in GJI2004 and EPSL2005 with additional uplift rate data compiled after that time, and compared the PDIMC effects based on the ice rate model used in EPSL2005 (UAF05), and an ice rate model based on *Larsen et al.* [2007] (UAF07). Although the viscosity values obtained by *Sato et al.* [2011] are within the associated uncertainty, the estimated asthenospheric viscosity is slightly larger by a factor of 1.5 or more than the previous values. The most likely reason for the difference in the obtained viscosity values is probably to be found in the differences in the magnitude of the estimated PDIMC effects in the respective studies. *Sato et al.* [2011] also examined the sensitivity of the uplift rate data in SE-AK to the viscoelastic structures of the upper and lower mantles,

[1]Research Center for Prediction of Earthquakes and Volcanic Eruptions, Tohoku University, Sendai, Japan.
[2]Key Laboratory of Computing Geodynamics, Graduate University of Chinese Academy of Science, Beijing, China.
[3]Earthquake Research Institute, University of Tokyo, Tokyo, Japan.
[4]Geophysical Institute, University of Alaska Fairbanks, Fairbanks, Alaska, USA.
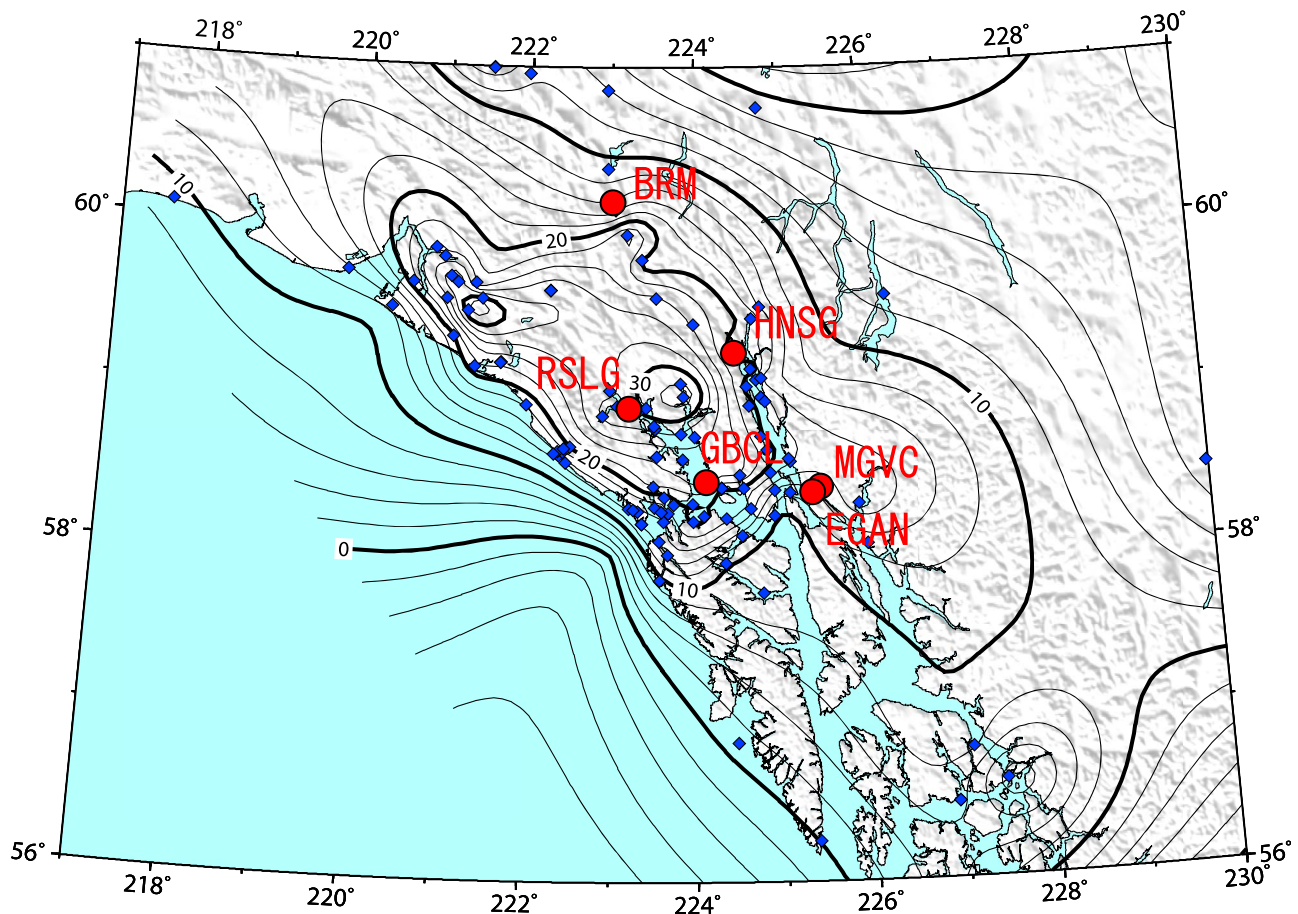
Figure 1. Absolute gravity sites of the ISEA project (red circles with station codes) and the contour map of the uplift rates (unit is mm/yr), which is produced using the vertical velocity rates observed at 143 GPS sites (blue diamonds).

and they conclude that the data is insensitive to the lower mantle viscosity.

[3] A U.S.-Japan joint observation project called ISEA [*Miura et al.*, 2007] was conducted during 5 years of 2006–2010. An AG network was established in 2006 by the project. The network consists of 6 sites in the GB area, SE-AK and in neighboring region of Canada. Details of the AG measurements by the ISEA project and the data processing are described by *Sun et al.* [2010]. The AG measurements provide useful data to discuss the long-term gravity changes, which should relate to the GIA processes, because the attraction part of the observed gravity changes is sensitive only to the effects of PDIMC and not to past mass changes. Therefore, there is a possibility to discuss the effects of the past and present ice mass changes more in detail by combining use the gravity data with the uplift data.

[4] *Wahr et al.* [1995] argued that the viscoelastic effects on the gravity rate due to such long-term deformations as Glacial Isostatic Adjustment (GIA) could be reduced by an order of magnitude by subtracting a term which is estimated from the product of the uplift rate multiplied by a coefficient of -0.154 μGal/mm, which is the sum of the Free-air gravity gradient of -0.308 μGal/mm and the Bouguer gravity gradient of $1/6.5$ μGal/mm that is related to the flow of the heavy mantle material into the rebounding area [*Fang and Hager*, 2001]. Therefore, the remaining part of the

observed gravity rates could be used to discuss the present-day thickness changes. *James and Ivins* [1998] applied the idea of *Wahr et al.* [1995] to predictions of Antarctic crustal motions driven by the PDIMC and by the GIA effects due to the LGM ice loss. *Sun et al.* [2010] used the similar approach to discuss the present-day ice thickness changes in SE-AK.

[5] AG measurements also were conducted in 1987 at two sites of the ISEA network [*Sasagawa et al.*, 1989]. In this paper, based on the uplift rate data in SE-AK, the gravity change rates obtained from the ISEA network and including the *Sasagawa et al.* [1989] data, we will discuss the results of a comparison of the observed gravity and uplift rates in SE-AK with the predicted rates obtained using three kinds of ice models for the three different ages of the LGM, the LIA and the PD. We will also discuss the viscous ratio of -0.154 μGal/mm mentioned above by comparing with the observed ratios.

2. Observed Data

[6] Figure 1 shows a contour map of uplift rates based on a set of newly reprocessed GPS solutions at 143 sites (blue diamonds) and the locations of 6 AG sites (red filled circles). These GPS solutions include a number of improved models compared to our earlier work, including the use of

Table 1. Six AG Sites of the ISEA Network in and Around the GB Area

Station Code	Longitude (deg)	Latitude (deg)	Height (m)
BRM	223.0079	60.1714 840	
HNSG	224.4653	59.2470	210
RSLG	223.2109	58.9064	210
GBCL	224.1251	58.4546	100
MGVC	225.4546	58.4168	80
EGAN	225.3600	58.3853	38

consistently reprocessed orbit and clock products from JPL, absolute phase center models, the GMF tropospheric mapping function [*Boehm et al.*, 2006], and ocean tidal loading models computed with the Earth center of mass reference frame [*Fu et al.*, 2011]. Based on *Argus et al.* [2010], the velocities are corrected for the estimated geocenter translation rate of ITRF. The coordinates of the 6 AG sites are shown in Table 1. Table 2 shows the GPS sites which are used for the comparison with the AG data.

[7] The AG observations were carried out using the same FG5 absolute gravimeter (i.e., FG5#111), which was manufactured by Micro-g LaCoste Inc. and is owned by the University of Colorado [*Bilham and Sasagawa*, 1994]. In order to reduce the effects of seasonal gravity variations, the observations were done at the same time of year (i.e., from late June to early July of each year). At each of the 6 AG sites, the gravity measurements were conducted over more than two days, with at least 100 sets acquired, including 100 free-fall drops per set. Thus the gravity value at each site was determined using the data more than 10,000 drops. The drop data were processed by the g-soft program provided by the manufacturer.

[8] Details of the AG measurements and the data processing are described by *Sun et al.* [2010].

2.1. Long-Term Gravity Changes at HNSG and BRM

[9] At the two sites BRM and HNSG, a group from IGPP at the University of California, San Diego had conducted AG measurements in 1987 with the AGM-1 gravimeter, a prototype of the FG5 absolute gravimeter [*Sasagawa et al.*, 1989]. Figure 2 shows the comparison between the 1987 AG data and our data. Based on a comparison measurement with an FG5 gravimeter, which was carried out in 1996 in California, *Sasagawa and Zumberge* [1997] estimated the systematic error (offset) of the AGM-1 to be 19 ± 1 μGal. First, this systematic error of AGM-1 was corrected by subtracting 19 μGal from the AG values given by *Sasagawa et al.* [1989]. Next, for consistency in the measuring height
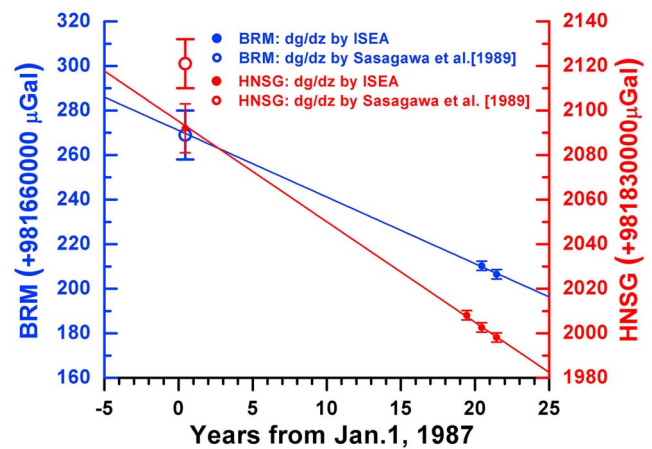

Figure 2. Long-term gravity changes observed at two AG sites of BRM and HNSG. Solid and open blue circles indicate AG values at BRM converted using the vertical gravity gradients measured by ISEA and by *Sasagawa et al.* [1989], respectively. Solid and open red circles indicate AG values at HNSG converted using the vertical gradients measured by ISEA and by *Sasagawa et al.* [1989], respectively. Blue and red lines are results for the fitting with least squares method.

with our AG values obtained with FG5#111 (i.e., 1 m above from the floor), we converted their values on the floor to those at the same height with us by using a measured vertical gravity gradient (unit: μGal/cm).

[10] The gravity gradient at each site was measured with a LaCoste–Romberg gravimeter (G-248) of UAF. In order to ensure the accuracy of the gravity gradient value used for the conversion, the final gradient values were determined from 6 pairs of round-measurements [*Sun et al.*, 2010]. The 1-σ formal error of the mean gravity gradient measured at each site is estimated to be at the order of ±0.01 μGal/cm (T. Sugano, personal communication, 2010). Table 3 compares the gravity gradients at the two sites of BRM and HNSG, which were measured by *Sasagawa et al.* [1989] and by the ISEA project. For BRM, the two gradient measurements agree within measurement error, but at HNSG they differ significantly. As shown in Figure 2, the AG values at BRM and HNSG measured in 1987 agree with the estimated linear trends, when we adopt the vertical gravity gradient measured by the ISEA project for HNSG instead of that given by *Sasagawa et al.* [1989]. The difference at BRM is small, because of the small difference in the gradient values between two measurements (see Table 3).

Table 2. GPS Sites Used in the Comparison With the AG Data[a]

| AG Site Code | GPS Site | | | | |
	Code	Span (years)	Longitude (deg)	Latitude (deg)	Distance (km)
BRM	MDFC4.1	223.04167	60.12182	5.82	
HNSG	HSSA_HNSD	8.8	224.46580	59.24810	0.20
RSLG	R205	9.3	223.21174	58.90540	0.12
GBCL	BCT5	3.1	224.11362	58.45407	0.67
MGVC	AB50	5.1	225.45470	58.41678	0.01
EGAN	JUN1	7.7	225.41430	58.36258	4.05

[a]Span indicates data span used in the analysis; distance indicates distance between the AG site and the GPS site.

Table 3. Comparison of the Vertical Gravity Gradients at HNSG and BRM

	HNSG (μGal/cm)	BRM (μGal/cm)
Sasagawa et al. [1989]	−2.80	−2.91
ISEA project	−3.093	−2.908

2.2. Observed Gravity Rates in SE-AK

[11] Table 4 shows a summary of the observed mean gravity values and rates at the 6 AG sites. As mentioned in the previous section, all gravity values are converted to those at the height of 1 m above from the floor. We reevaluated the gravity rates by using the uncertainties as a weight of the fitting. The difference in the treatment of errors in the fitting is a reason for the difference in the gravity rates shown by *Sun et al.* [2010, Table 3] and Table 4. However, the difference between two estimations is less than 0.1 μGal/yr at all AG sites. The mean gravity rates over the 6 sites are −4.50 ± 0.76 μGal/yr and −4.30 ± 0.92 μGal/yr for the cases of only using the data obtained in the period of 2006–2008 and simultaneously using the data in 1987 with our data, respectively.

3. Model Computations

3.1. PDIMC Models and Effects of PDIMC

[12] Accuracy of the estimation of PDIMC effects affects the discussion of the viscoelastic effects based on the observed rates [e.g., *Sato et al.*, 2006]. The computation method used here is similar to that described by *Sato et al.* [2011]. Thus, according to *Farrell* [1972], we estimated the effects of PDIMC on the observed gravity and uplift rates by convolving the ice mass loads with the elastic loading Green's function over the glacier masses. Computations are done using a modification of a program code called 'GOTIC' [*Sato and Hanada*, 1984]. Unlike the effects of past ice loss, in the gravity effects of PDIMC, we should consider not only the effects of the elastic deformation but also the changes in the Newtonian attraction due to the ice mass changes. The computation for the attraction part is sensitive to the relative locations of the observation site and the loading mass. We took this into account in the convolution integral using the elevation data given in the ETOPO2 digital elevation model (http://www.ngdc.noaa.gov/mgg/

global/etopo2.html) as the ice surface elevations, and we computed the effects of the thickness change (m/yr) at the height of each grid point given by the PDIMC models.

[13] An advantage of the integration method used in GOTIC is that we can avoid a singularity in the convolution for the case in which the locations of the observation site and the loading point are the same. This is important to maintain the computation accuracy, especially for the Newtonian attraction part. The grid size of the ice model discretization also contributes to the computation errors. The original ice mass loss rate data were averaged with a longitude–latitude grid of 0.083° by 0.042°, so that each grid is approximately a 4.6 km by 4.7 km square (at 60°N latitude). The Green's functions of the orders up to 10,000 in harmonic degrees are used for the computations. So, the minimum loading distance represented with the Green's function is about 0.036°, smaller than the grid size of 0.042°. The Green's functions for the Earth model PREM [*Dziewonski and Anderson*, 1981] are used in the computation.

[14] *Sato et al.* [2011] discussed the sensitivity of the estimated uplift rates to the PDIMC models. We also tested this for the gravity rates. Two present-day ice mass-loss rate compilations, which are respectively called here the UAF05 and UAF07 models, are used for the test. UAF05 was constructed mainly based on *Arendt et al.* [2002], and it was also used in GJI04 and EPSL05. UAF07 was obtained from differencing two digital elevation maps (DEMs): the 2000 Shuttle Radar Topography Mission (SRTM) and the USGS NED DEM based on aerial photos dating from 1948 to 1987 [*Larsen et al.*, 2007]. The UAF07 model is based on a more complete elevation change data set, with less regional extrapolation than UAF05. In addition, there is a difference of about 15 years in the mean epochs between two PDIMC models, with the UAF07 model including more recent data.

3.2. The Past-Ice Mass Change Models and Their Effects

3.2.1. Effects of LIA Ice Loads

[15] The effects of unloading after the LIA are estimated basing on the melting history described in GJI04 and EPSL05. At the peak of the LIA, the GB area was covered with glaciers more than 1.5 km in thickness (e.g., EPSL05). Glaciers began to wane after the peak of the LIA in the middle of the 18th century, and this thick ice coverage in Glacier Bay underwent a rapid retreat [e.g., *Molnia*, 2008;

Table 4. Observed Gravity Values and the Gravity Rates at the Six AG Sites[a]

Site	Mean Gravity Value[b] (μGal/yr)	Uncertainty (μGal)	Precision (μGal)	Rate (μGal/yr)	Error
BRM	981660208.39	2.09	0.23	−3.79 (−2.99[c])	xxx (0.53[c])
HNSG	981832002.94	2.10	0.26	−4.92 (−4.50[c])	1.46 (0.52[c])
RSLG	981796820.00	2.13	0.59	−3.46	1.51
GBCL	981768405.39	2.09	0.35	−5.54	1.46
MGVC	981745276.79	2.10	0.28	−4.62	1.53
EGAN	981760216.29	2.11	0.41	−4.67	1.53
Mean	981760488.30	2.10	0.35	−4.50 (−4.30)	
SD	±57938.31	±0.02	±0.13	±0.76 (0.92)	

[a]SD is the standard deviation of the mean.
[b]Mean gravity value for the 3 years from 2006 to 2008.
[c]The gravity rates obtained by simultaneously using the gravity data in 1987 [*Sasagawa et al.*, 1989] and our data for the 3 years. Error of "mean" shows the standard deviation of the mean value. Three crosses indicate that the error of this case is not estimated, because the rate of BRM is determined only using 2 data in 2006 and 2007.

Table 5. Earth Models Used in This Study

Layer	Radius (10^6 m)	Density (10^3 kg m^{-3})	Shear Modulus (10^{11} Pa)	Viscosity (10^{21} Pa s)
		Two-Layer Viscoelastic Model[a]		
0	3.480	10.930	0.0000	0.00000
1	6.207	4.535	1.8330	0.40000
2	6.317	3.373	0.6719	0.00558
3	6.371	3.028	0.5253	infinity
		Four-Layer Viscoelastic Model[b]		
0	3.480	10.930	0.00000	0.000
1	5.701	4.878	2.19490	2.000
2	5.971	3.858	1.06480	0.400
3	6.151	3.476	0.76495	0.400
4	6.311	3.370	0.66830	0.010
5	6.371	3.028	0.52530	infinity

[a]Averaged PREM with 110 km thick asthenosphere, 20 <= LT <= 120 km. Lithospheric thickness is 54.0 km.
[b]Thickness of PREM- averaged mantle model. Elastic lithosphere is 60 km, shallow upper mantle 1 is 160 km, shallow upper mantle 2 is 180 km, transition zone is 270 km, and lower mantle is down to the CMB.

GJI04; EPSL05]. As shown in Figure 8A of GJI04 and Figure 5A of EPSL05, their loading models for the post-LIA period consists of two kinds of ice loads, five disks for the GB load of the diameter of 0.4° or 0.8° and 531 disks of mean diameter 0.2° for the other regional glaciers and ice fields in SE-AK. The regional model includes the recent accelerated wastage starting on around 1995 [*Arendt et al.*, 2002].

[16] The computations were done using a computing code called 'TABOO," which is based on an incompressible GIA modeling with a layered Maxwell body [*Spada et al.*, 2003, 2004]. We assume here that, for both GJI2004 and EPSL2005, all of the loadings by the post-LIA ices were terminated to zero in the year 2000, and we computed the unloading effects in the year 2005, so that the computational results do not include the effects of elastic deformation and the change in the Newtonian attraction due to the past loads, because these effects were computed separately with the PDIMC model. The original TABOO code does not include the computing routine for the time variation in gravity anomaly $g(t)$ and its time derivative $\delta g(t)$. We compute $g(t)$ and $\delta g(t)$ by referring to *Peltier* [1974, equation (65)], which represents the viscous parts of the impulse response for the gravity anomaly, and by using the related quantities obtained by the TABOO code, for example, the time convolutions and their time derivatives between the load Love numbers $h_n(t)$ and $k_n(t)$ of the harmonic degree n and the melting history of each of the 536 disk loads. As shown by *Sato et al.* [2011, Figure 4], the computation results for the convolution integral almost reach to its final value at around the harmonic degree of 130. For safety, we also used a maximum harmonic degree of 480.

3.2.2. Effects of Post-LGM Unloading

[17] The effects of post-LGM ice unloading were computed using the ICE-3G model [*Tushingham and Peltier*, 1991] and using the modified TABOO code explained in the previous section. As with the effects of LIA, we computed the viscoelastic effects in 2005 AD. The effects of the LGM are small in SE-AK for both the uplift and gravity. At any of the 6 AG sites, the model rates are on the order of

1–2 mm/yr for the uplift rates and less than 1 μGal/yr for the gravity rates. SE-AK is located far from the main Laurentide ice sheet, and the Cordilleran ice sheets in SE-AK had mostly melted by 8 ky BP. This is a completely different situation from the Hudson Bay region [e.g., *Sella et al.*, 2007]. The small magnitude of the effects of LGM also means that the differences between different GIA models are not significant for this region.

3.3. Results for Model Computations

[18] We have compared two kinds of the viscoelastic Earth models. One is the 2-layer model used in the papers by GJI2004, EPSL2005 and *Sato et al.* [2011], and the other is a model having 4 viscoelastic layers. The layered parameters are shown in Table 5 for the 2-layer model and the 4-layer model. Table 6 compares the χ^2 values of the residuals for the GPS data by obtaining from the different combinations of the two Earth models of the 2-layer and 4-layer and the PDIMC ice loss models of UAF05 and UAF07. As shown in Table 6, the χ^2 values obtained using the 4-layer model are smaller than those obtained using the 2-layer model in all cases using UAF05 and UAF07 models. So we use here the results obtained by the 4-layer model in our discussions. The density and elastic structure of the model are taken from PREM.

[19] As shown in Table 6, the magnitude of the estimated χ^2 of the residuals depends on not only the viscoelastic Earth model but also the PDIMC model used in the computations. Therefore, we also examine the sensitivity of the observed gravity rates to the PDIMC models. Table 7 shows the comparisons between the observed uplift rates and the model predictions using the UAF05 and UAF07 models. Table 8 shows the comparison results for the gravity rates.

3.4. Estimation of Viscous Ratios

[20] We estimated the viscous portion of the ratio of the observed gravity rate to the uplift rate (unit: μGal/mm) by removing the computed PDIMC effects from the observed rates (hereafter we call the corrected ratio the "viscous ratio"). Table 9 shows the viscous ratios which were obtained by correcting for the PDIMC effects using the UAF05 model or the UAF07 model.

[21] Figure 5 plots the observed viscous ratios at the 6 AG sites given in Table 9 with the model values. Six kinds of the viscous ratios are plotted; (1) Blue filled circles: the viscous ratios corrected using UAF05, (2) Red filled circles: the ratio corrected using UAF07, (3) Blue open circle: the mean of (1), (4) Red open circle: the mean of (2), (5) Green open circle: the ratio estimated using both the LGM and LIA ice models, and (6) Purple filled circle: the ratio estimated only

Table 6. Changes in χ^2 Values of the Residuals for the GPS Uplift Data by the Difference in the Combinations of the Viscoelastic Earth Model and the PDIMC Model

Earth Model	PDIMC Model	χ^2
Two-layer	UAF05	2.629
Two-layer	UAF07	1.480
Four-layer	UAF05	2.439
Four-layer	UAF07	1.349

Table 7. Comparison Between the Observed Uplift Rates and the Predicted Rates

AG/GPS	PDIMC (mm/yr)	LIA (mm/yr)	LGM (mm/yr)	Sum (mm/yr)	Observation (mm/yr)	Error (mm/yr)	Residual (mm/yr)	Contribution of PDIMC (%)
				PDIMC Model: UAF05				
BRM/MDFC	2.88	13.37	0.77	17.02	16.16	0.01	−0.86	17.6
HNSG/HNSA_HNDS	3.24	17.09	0.88	21.21	23.05	0.15	1.84	14.1
RSLG/R205	4.78	21.47	0.68	26.93	30.03	0.22	3.10	15.9
GBCL/BCT5	2.58	15.98	0.76	19.32	26.09	0.48	6.77	9.9
MGVC/AB50	2.81	11.05	0.93	14.79	15.31	0.03	0.52	18.4
EGAN/JNU1	2.55	11.20	0.91	14.66	14.49	0.04	−0.17	17.6
Mean							1.87	15.6
SD							±2.79	±3.2
				PDIMC Model: UAF07				
BRM/MDFC	3.63	13.37	0.77	17.77	16.16	0.01	−1.61	22.5
HNSG/HNSA_HNDS	5.41	17.09	0.88	23.38	23.05	0.15	−0.33	23.5
RSLG/R205	5.24	21.47	0.68	27.39	30.03	0.22	2.64	17.4
GBCL/BCT5	3.74	15.98	0.76	20.43	26.09	0.48	5.61	14.3
MGVC/AB50	4.74	11.05	0.93	16.72	15.31	0.03	−1.41	31.0
EGAN/JNU1	4.53	11.20	0.91	16.64	14.49	0.04	−2.15	31.3
Mean							0.46	23.3
SD							±3.05	±6.9

using the LIA ice model. The error of the observed viscous ratios was estimated basing on the errors shown in Tables 7 and 8 for the uplift rates and the gravity rates, respectively.

4. Discussions

4.1. Observed Gravity Rates

[22] Figure 2 indicates (1) the high reliability of the AG measurements for detection of the long-term gravity changes due to GIA, (2) the importance of examining precisely the systematic error in the AG instruments and (3) the importance of measuring the vertical gravity gradient as precisely as possible in order to determine the long-term gravity rate from the data obtained from AG instruments with the different measuring height and at different times.

4.2. Comparison of Observed Rates With Model Predictions

[23] Figures 3a and 3b plot the uplift rates shown in Table 7. Figures 3c and 3d plot the gravity rates shown in Table 8. Except for 1 or 2 sites (the number depends on the components), the model predictions recover both the uplift and gravity rates observed from the AG and GPS within their mean observation errors (i.e., ±2.1 μGal/yr and ±2.3 mm/yr, respectively) as the sum of the effects of ice loss using the three kinds of ice models for the ages of LGM, LIA and PD.

[24] The mean values of the residuals, which are shown in the column named 'Mean' of Tables 7 and 8, indicate that the magnitude of the mean values is clearly improved by using UAF07 model instead of UAF05 (i.e., 4.1 and 3.5 times

Table 8. Comparison Between the Observed Gravity Rates and the Predicted Rates

AG Site	PDIMC (μGal/yr)	LIA (μGal/yr)	LGM (μGal/yr)	Sum (μGal/yr)	Observation (μGal/yr)	Error (μGal/yr)	Residual (μGal/yr)	Contribution of PDIMC (%)
				PDIMC Model: UAF05				
BRM	−0.45	−2.27	−0.06	−2.78	−2.99[a]	0.53[a]	−0.21	15.1
HNSG	−0.45	−2.92	−0.06	−3.43	−4.50[a]	0.53[a]	−1.07	10.0
RSLG	−2.04	−3.67	−0.05	−5.76	−3.46	1.51	2.30	59.0
GBCL	−0.51	−2.73	−0.07	−3.31	−5.54	1.46	−2.23	9.2
MGVC	−1.36	−1.88	−0.09	−3.33	−4.62	1.53	−1.29	29.4
EGAN	−0.82	−1.91	−0.09	−2.83	−4.67	1.53	−1.85	17.6
Mean							−0.59	25.3
SD							±1.66	±17.9
				PDIMC Model: UAF07				
BRM	−0.55	−2.27	−0.06	−2.88	−2.99[b]	0.53[b]	−0.11	18.4
HNSG	−1.65	−2.93	−0.06	−4.64	−4.50[b]	0.53[b]	0.14	36.7
RSLG	−1.12	−3.67	−0.05	−4.68	−3.46	1.51	1.38	32.4
GBCL	−0.78	−2.73	−0.07	−3.58	−5.54	1.46	−1.96	14.1
MGVC	−2.65	−1.88	−0.09	−4.62	−4.62	1.53	0.00	57.4
EGAN	−2.22	−1.91	−0.09	−4.22	−4.67	1.53	−0.45	47.5
Mean							−0.17	34.4
SD							±1.08	±16.6

[a]Results obtained by simultaneously using our data for 3 years with the data in 1987 by *Sasagawa et al.* [1989].
[b]Rates and their errors obtained by simultaneously using our AG data for 3 years with the data in 1987 by *Sasagawa et al.* [1989].

Table 9. Comparison of the Viscous Ratios[a]

AG Site	GPS Site	Distance (km)	Gravity Rate (μGal/yr)		Uplift Rate (mm/yr)		Ratio (μGal/mm)	
			UAF05	UAF07	UAF05	UAF07	UAF05	UAF07
BRM	MDFC	5.82	−2.54	−2.44	13.28	12.53	−0.192 (0.040)	−0.195 (0.042)
HNSG	HNSA_HNDS	0.13	−3.60	−2.85	19.81	17.64	−0.182 (0.023)	−0.162 (0.026)
RSLG	R205	0.12	−1.42	−2.34	25.25	24.79	−0.056 (0.059)	−0.094 (0.059)
GBCL	BCT5	0.67	−5.03	−4.76	23.51	22.35	−0.214 (0.042)	−0.213 (0.046)
MGVC	AB50	0.01	−3.26	−1.97	12.50	10.57	−0.261 (0.122)	−0.187 (0.145)
EGAN	JNU1	4.05	−3.85	−2.45	11.94	9.96	−0.322 (0.128)	−0.246 (0.153)
Mean			−3.36	−2.80	17.72	16.31	−0.205	−0.183
SD			±1.26	±1.00	±5.92	±6.29	±0.089	±0.052

[a]Two cases are compared, which were obtained by correcting the PDIMC effects with the UAF05 and UAF07 models, respectively. Distance indicates distance between the AG site and the GPS site. Value in parentheses shows the error of the estimated viscous ratio.

in the mean magnitudes of residuals for the uplift and gravity, respectively). Since, in general, a small mean value of the residuals may reflect a small systematic error, it suggests that the model predictions using UAF07 are much more consistent with the observations than those using UAF05.

[25] The major difference between the two models is that UAF07 is based on a much more complete set of elevation changes, and requires much less regional extrapolation than UAF05. Moreover, the difference in the mean epoch of the ice data used to construct respective models may contribute.

Since UAF07 is younger than UAF05 by about 15 years, UAF07 represents the effects of PDIMC that are much closer to the present-day than UAF05. The difference in the gravity rates at the two sites BRM and HNSG shown in Table 4 suggestive that it does. At both sites, the gravity rates estimated from the recent data for the period of 2006–2008 are slightly larger (by about 5%) than those obtained from the data over the past 20 years.

[26] As shown in the column named 'Contribution of PDIMC' of Tables 7 and 8, for any cases of the uplift and
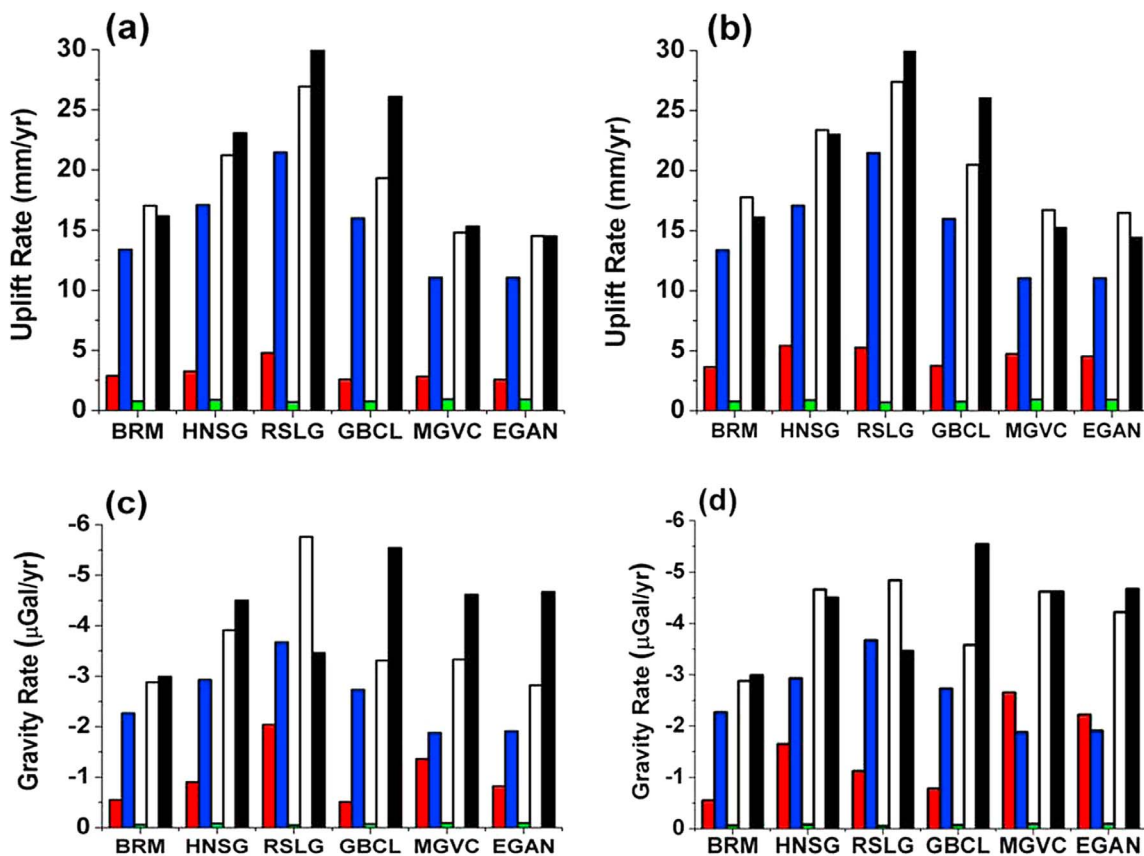

Figure 3. Comparison between the observed rates and the computed rates at six AG sites. (a and c) Uplift rates and gravity rates estimated using the UAF05 model as the PDIMC model, respectively. (b and d) The cases using the UAF07 model. In each plot, red bars indicate the effect of PDIMC, blue bars indicate the effect of LIA, green bars indicate the effect of LGM, white bars indicate the sum of these three effects, and black bars indicate observations.
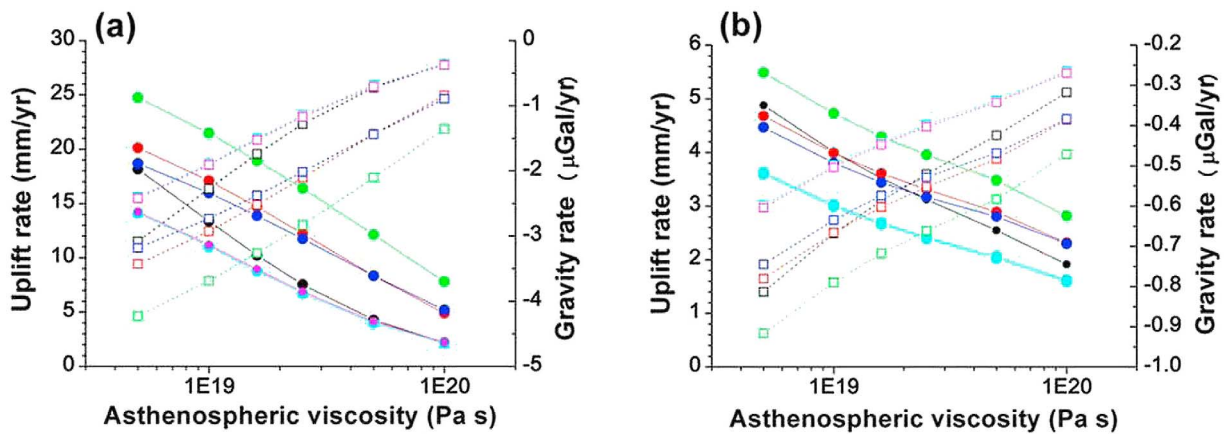
Figure 4. Effects of the lithospheric thickness and the asthenospheric viscosity on the computed gravity rate and the uplift rate. The computation results for the unloading of LIA ices are shown. (a) Results for the case of lithospheric thickness of 60 km. (b) Results for the case of lithospheric thickness of 120 km. The solid lines with the solid circles and the dotted lines with the open squares show the uplift rates and the gravity rates, respectively. Black, BRN; red, HNSG; green, RLSG; blue, GBCL; light blue, MGVC; and purple, EGAN.

gravity and for all sites, the magnitudes of the contributions of PDIMC estimated using UAF07 is larger than those using UAF05. On average, the contributions of PDIMC effects are 16% and 23% of the observed uplift rates and 25% and 34% of the observed gravity rates for the cases using UAF05 and UAF07, respectively. The differences in the magnitudes of the contributions and the residuals mentioned above indicate that the GPS and AG observations surely detect the recent increase of the ice mass loss in SE-AK. On the other hand, the difference in the magnitude of the contribution of PDIMC between the uplift rates and gravity rates may show the high sensitivity of the gravity due to the contribution of its attraction part.

[27] From the comparisons between the observations and the model predictions, we can say that the rates detected from the AG and the GPS are consistent with each other, even though the effects of the ice changes are different between the two observations. However, for both the uplift and gravity, a relatively large difference between the observations and the predictions, especially in the gravity rate, is observed at GBCL. The exact reason for it is not clear yet, but, as pointed out by *Sun et al.* [2010], the error in the PDIMC models is probably one of the error sources in this study, because recently very rapid glacier retreat is observed in Alaska including SE-AK [e.g., *Larsen et al.*, 2009; *Luthcke et al.*, 2008]. We will discuss about other possible reason in section 4.5.

4.3. Lithospheric Thickness and Asthenospheric Viscosity in SE-AK

[28] Our previous studies based on uplift data [GJI04; EPSL05; *Sato et al.*, 2011] require a thin lithosphere and a low asthenospheric viscosity beneath SE-AK to explain the observed large uplift rates there. Since, as shown in Figure 3, the viscoelastic effects of post-LIA ice loss are far larger than the effects of the LGM, we examined the sensitivities of the computed gravity rates to the lithospheric thickness and the asthenospheric viscosity based on the post-LIA ice model, and compare with the uplift rates.

[29] Figures 4a and 4b show examples of the results for the sensitivity tests. Here, Figures 4a and 4b show the two cases respectively obtained assuming 60 km and 120 km as the thickness of the lithosphere. For the viscosity changes, both the obtained uplift and gravity rates are monotonically decreasing with an increase of the assumed asthenospheric viscosity. On the other hand, for the thickness of lithosphere, as shown by *Sato et al.* [2011, Figure 8], the χ^2 values rapidly increase at the ranges exceeding 60 ± 10 km. Corresponding to this, the comparison between Figures 4a and 4b clearly indicates that 120 km is too thick for any athenospheric viscosities tested here to explain either of the observed gravity rates and the observed uplift rates. Moreover, the results shown in Figure 4 and Table 8 indicate that the rheological structure beneath SE-AK inferred from the GPS data is also a good model for the gravity data.

4.4. Observed Viscous Ratio in SE-AK

[30] As shown in Figure 5, the scatter of the viscous ratio estimates using the UAF07 model is remarkably reduced compared with that obtained using the UAF05 (by a factor of ∼2). The mean values of the model viscous ratios are -0.166 μGal/mm and -0.171 μGal/mm for the cases estimated using two effects of the LIA and LGM and only using the effects of the LIA, respectively. The mean values obtained from the model computations are closer to the ratio estimated from the observed rates corrected using the UAF07 PDIMC model rather than that using the UAF05 model, although they are within overlapping error ranges.

[31] The estimated viscous ratios in SE-AK are sensitive to not only the PDIMC model used for the correction but also to the distance between the AG site and the GPS site used for the comparison, because of the large spatial gradient of the uplift rates. For example, for the GBCL AG site, the ratio changes from -0.21 μGal/mm to -0.29 μGal/mm, if we use the GUS2 GPS site (distance: 11 km) instead of BCT5 (distance: 0.67 km) that is used here. Using the uplift rate at BCT5 gives a value that is in better agreement with
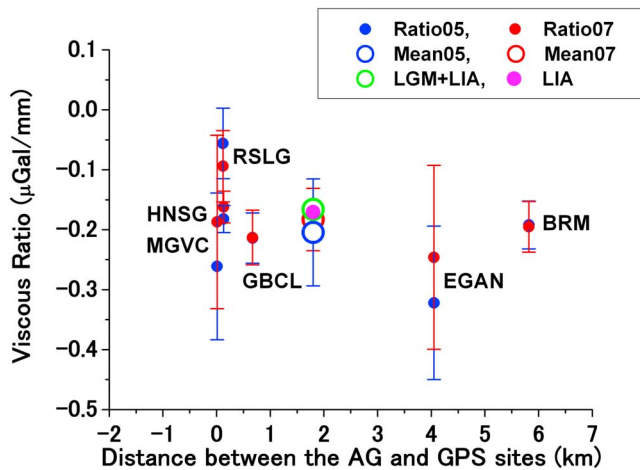
Figure 5. Comparison of the viscous ratios corrected using two PDIMC models of UAF05 and UAF07. Six kinds of the viscous ratios are plotted: (1) blue solid circles, the observed viscous ratios corrected using UAF05; (2) red solid circles, the observed ratio corrected using UAF07; (3) blue open circle, the mean of the blue solid circles; (4) red open circle, the mean of the red solid circles; (5) green open circle, the ratio estimated using both the LGM and LIA ice models; and (6) purple solid circle, the ratio estimated only using the LIA ice model.

other sites, and consequently the variance of the mean viscous ratio is improved.

[32] Figure 6 shows the predicted time variation of the viscous ratios between 2005 and 12,005, computed using the melting history of the post-LIA model. The viscous ratios increase with time, and they approach -0.154 μGal/mm. As described in section 3.2.1, our computation of the visco-elastic effects using the TABOO code is based on the Maxwell model and incompressible Earth. A possible reason for the consistency between -0.154 μGal/mm and our value at around 12005 AD may be due to a property of the Maxwell body, pointed out by *Fang and Hager* [2001]. *Fang and Hager* [2001] concluded that the non-elastic response of the Earth is nearly incompressible for the Maxwell Earth.

[33] Regarding the effect of the Earth's compressibility, *Tanaka et al.* [2009] examined its effect on the computation of surface loading. Their results for the comparison between the compressible and incompressible cases indicate; (1) The difference in the horizontal component is larger than that in the vertical component, (2) In the time rates of the Love numbers h and k, which relate to the vertical components, the differences are dominant for the integration time within 1–3 kyr, (3) The differences quickly decrease with a lapse of time for any spherical harmonic degrees between $n = 2$ and 150 that they tested, and (4) For the time range larger than 10 kyr, the differences between two cases are less than 10% [see *Tanaka et al.*, 2009, Figure 4d]. Figure 6 may reflect these conditions.

[34] Since the effects of the compressibility depend on not only the integration time but also on the harmonic degrees, it is not easy to say the magnitude of the effects of compressibility in our case, however, there is a possibility that ignoring the effect of the Earth's compressibility may make an error at the order of 10–25% in our model estimations.

Related to this, it may be worthwhile to note that the effects of compressibility are dominant in the early stage of the relaxation of the loading. The computation with the compressible Earth model may be important on our estimation of the PDIMC effects.

[35] For the model computation, the TABOO code used here does not treat the components of the degrees 1 [*Spada*, 2003]. As well as the effects of the compressibility, the difference between the case with the degree 1 component and that without it is dominant in the early stage of the relaxation [*Spada et al.*, 2011]. Improving model computations, which are taken into account the compressibility of the Earth and the degree 1 harmonics, are a remaining problem for further study.

4.5. Effects of the Seasonal Changes in Hydrology and Cryo-Sphere

[36] The seasonal effects due to the changes in hydrology and cryo-sphere, which are not corrected here, should be an error source in our discussions based on the data that were mainly obtained from observations made in a campaign style. In order to reduce these effects, most of the AG and GPS measurements were carried out during the summer season. Especially, the AG observations, which are sensitive to the position of the mass, were carried out at the same time of each year (i.e., from late June to early July of each year).

[37] As an example, Figure 7a shows the time series of the displacements observed at the Plate Boundary Observatory continuous GPS (CGPS) site AB50, which is used for the comparison with the AG observation at the MGVC site. Both sites are located beside the Mendenhall glacier (distance: about 2 km) and the Mendenhall lake (distance: about 0.4 km). We observe in Figure 7a clear seasonal changes in the vertical displacement with an amplitude of about 24 mm in peak-to-peak. For the data of CGPS, the trend component was estimated by fitting a model that consists of the three components of the annual, semiannual and linear trend. We obtain 11.47 ± 0.22 mm and 273.2 ± 1.1 degrees for the annual amplitude and phase at AB50. Thus, the plus and minus peaks of the annual change appear at the early autumn and the early spring, respectively. Figure 7a indicates also
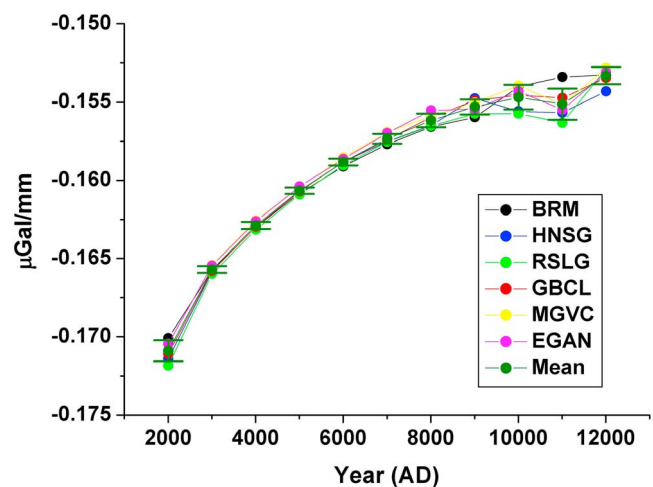

Figure 6. Time variation of the viscous ratios computed using the unloading effects of the LIA ices.
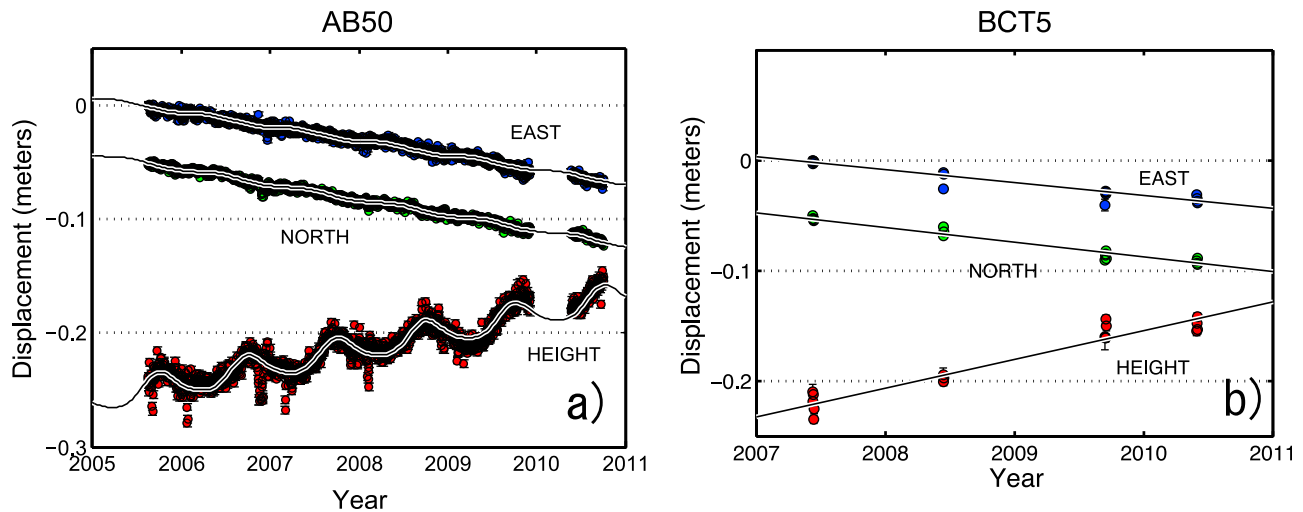
Figure 7. (a) Example of the time series of displacements observed at a continuous GPS site AB50, which is used to compare the MGVC AG site. These sites locate beside the Mendenhall glacier and the Mendenhall Lake. (b) Example of the plot of the displacement data obtained at a campaign GPS site BCT5, which is used to compare the GBCL AG site.

that the observed seasonal amplitudes are almost stable over the period of 5 years. Similar tendencies are observed at other CGPS sites. Related to this, the GRACE mascon solutions by *Luthcke et al.* [2008] show a good spatial coherency in the phases of the seasonal mass changes in the glacier regions of the Gulf of Alaska [see *Luthcke et al.*, 2008, Figure 3].

[38] Figure 7b plots the data at a campaign site BCT5, which is used for the comparison with the AG observation at the GBCL site. As expected from Figure 7a, the deviations of the observed height data from the fitted linear curve are small for the data obtained in the middle of each year. The data for the vertical component in 2009.7 show a relatively large shift by about 13 mm to the positive direction. It is an effect of the seasonal variations, as the measurements were made closer to the peak seasonal uplift. As indicated by the formal 1-σ error of the estimated uplift rates shown in the column named 'Error' of Table 7, possible systematic errors due to the effects of non-corrected seasonal variations are remarkably reduced by our observation strategy and by using the data obtained over 4 years or more than it. However, as shown in Table 2, compared with other sites, the data span of the GPS measurements at BCT5 is 3.1 years. This short data span and the seasonal effects shown in Figure 7b may contribute to the relatively large differences between the observation and the model prediction at GBCL as well as the case of the gravity measurements. In order to figure out the definite reason of the difference at GBCL, it is necessary to conduct more AG and GPS measurements.

[39] *Lambert et al.* [2006], who analyzed the AG data obtained over nearly a decade at 10 sites in North America, found that the seasonal variations are very small at a site which satisfies the following conditions: (1) a rocky environment, where the soil does not saturate, and (2) the proximity to the ocean, where rapid run-off of the soil moisture is expected. RSLG and GBCL satisfy both these conditions. Figure 2 indicates that the systematic errors at BRM and HNSG due to the effect of the seasonal variations on our

estimation of the gravity rates may be less than the observation errors; the data in 1987 were obtained during the same season (i.e., June).

4.6. Effects of Tectonic and Post-Seismic Deformations

[40] It is known that SE-AK is a tectonically active area. However, the tectonic effect is expected to be small in the vertical component. In most of the study area, the vertical tectonic deformation has to be much smaller than the deformation due to the GIA, because the area is dominated by strike-slip motions [*Elliott et al.*, 2010]. In fact, for most of the AG sites used in this study, the vertical velocities are several times larger than the horizontal ones. Although the post-seismic effects of the 1964 earthquake of $M_w9.2$ are large within its rupture zone and above the mantle wedge of the subduction zone, the area shown in Figure 1 is more than 400 km away from the end of the rupture zone and is far from the mantle wedge. The values for the shear modulus and the viscosity of the asthenosphere used here and in post-seismic studies are not so different [e.g., GJI2005; EPSL2005; *Sato et al.*, 2011; *Suito and Freymueller*, 2009; *Ali and Freed*, 2010]. If we use the values shown in Table 5, the relaxation time in SE-AK is estimated to be at the order of 3 to 5 years. This short relaxation time means the post-seismic deformation related to earthquakes in SE-AK will decay rapidly. The distance from the 1964 earthquake makes its effect small here.

[41] Using a 3-D viscoelastic finite element model, *Suito and Freymueller* [2009] computed the effects of the viscoelastic and afterslip postseismic deformations following the 1964 Alaska earthquake. Figure 8 shows the contour maps of the horizontal rates (Figure 8a) and the vertical rate (Figure 8b), which are based on the numerical data obtained by *Suito and Freymueller* [2009] (J. Freymueller, personal communication, 2011). Although the SE-AK area is not included in their model computations, the contour maps indicate that the rates related to the post-seismic deformation in our study area are smaller than 1 mm/yr and 0.5 mm/yr for
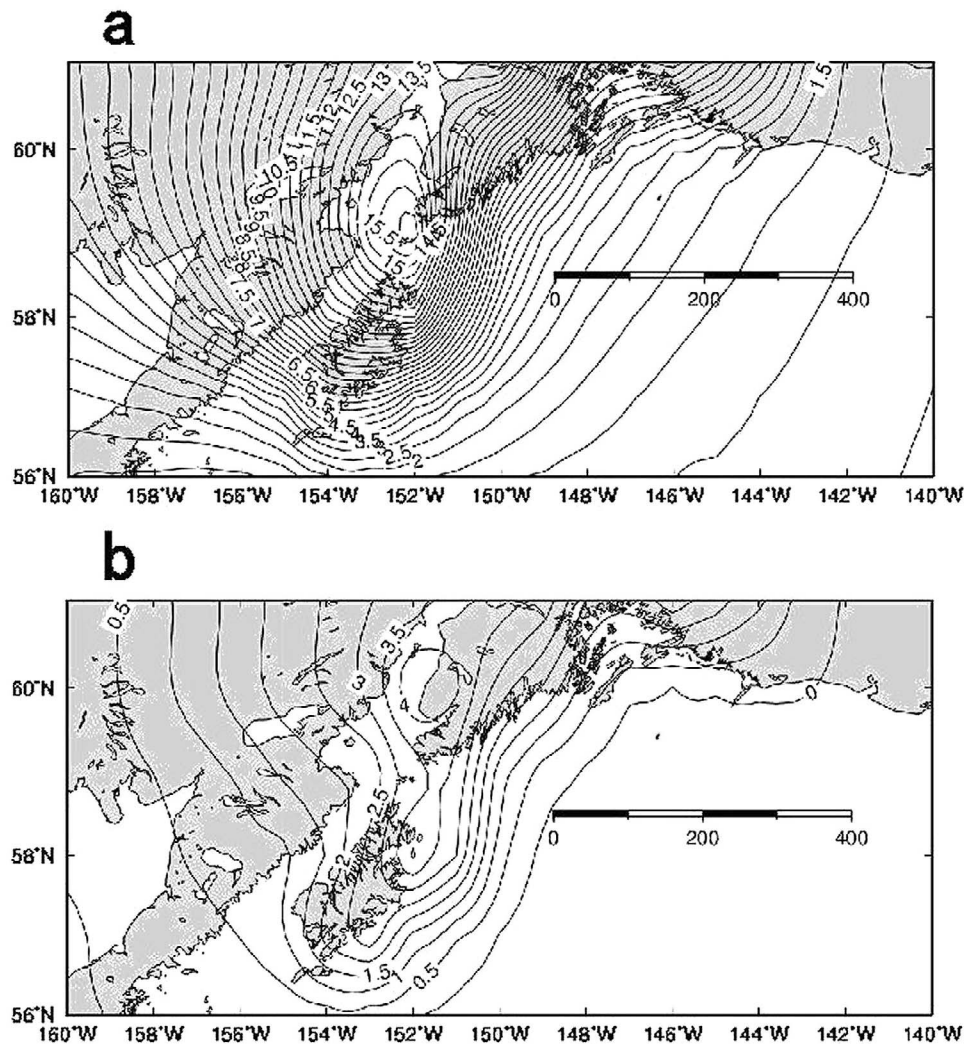
Figure 8. Post-seismic displacements caused by the 1964 Alaska earthquake of M9.2. The contour maps of (a) the horizontal rates and (b) the vertical rates. The data are taken from the model computations by *Suito and Freymueller* [2009]. Black and white bar shows the horizontal scale in km.

the horizontal and vertical components, respectively. Using also the 3-D viscoelastic Finite Element Model, *Ali and Freed* [2010] estimated the horizontal rates in Southern Alaska (including the area of SE-AK) due to the contemporary deformations associated with the four large events prior to the 2007 M7.9 Denali quake. According to *Ali and Freed* [2010, Figure 2], except for the Yakutat block, the horizontal rates obtained by combing the three deformations of the interseismic, the viscoelastic relaxation and the afterslip are estimated to be at the order of 2 mm/yr in amplitude in SE-AK. In this connection, the amplitude of 2 mm/yr for the horizontal rate is consistent in magnitude with the velocity of the GB block estimated by *Elliott et al.* [2010], which was obtained from the GPS data by correcting for the GIA effects.

[42] If we take the ratio of the vertical displacement rates to the horizontal ones of the data by *Suito and Freymueller* [2009], we obtain a value of 0.24. Using this ratio and the horizontal rate of 2 mm/yr by *Ali and Freed* [2010] gives a rate of 0.48 mm/yr as the uplift rate due to the effect of the seismic deformations in SE-AK. If we use a value of

-0.1933 μGal/mm for the Bouguer corrected gravity gradient to the vertical crustal motion (i.e., -0.3086 μGal/mm for the Free-air gradient and $+0.1153$ μGal/mm for the Bouguer gradient with a crustal density of 2750 Kg^1 m^{-3} (granite)) and the vertical rate of 0.48 mm/yr, we obtain a gravity rate of -0.09 μGal/yr as the effect of the post-seismic deformations.

[43] If we systematically subtract these rates from the uplift and gravity rates corrected for the PDIMC effects shown in Table 9, we obtain the viscous rates of -0.206 ± 0.092 and -0.183 ± 0.053 in unit of μGal/mm for the cases respectively using the PDIMC models of UAF05 and UAF07. These ratios are almost same in magnitude as those shown in Table 9; the difference is less than 1% of the value.

4.7. Effects of the Oceans

[44] Among the effects of the oceanic variations, those of ocean tide loading (OTL) are significant signals in both the AG and GPS observations in SE-AK. Errors in the OTL models will cause an error in the observed rates, because most sites are located within a few km from the coast and

most of our data were obtained from the campaign observations. The OTL models based on open ocean tide data from the satellite altimetry poorly predict tidal effects in SE-AK, due to the complex topography and bathymetry and long glacial fjords [*Sato et al.*, 2008; *Inazu et al.*, 2009]. The OTL models built into the g-soft program share the same limitation. *Sun et al.* [2010] show that using a newly developed regional ocean tide models [*Inazu et al.*, 2009] for the correction remarkably improves the SD of the set gravity residuals (by more than 50%). Improvement likely could be made in the GPS time series used in this study, although the effects are most likely smaller.

[45] Global sea level changes also affect our uplift and gravity rates. *Church and White* [2011] analyzed satellite altimeter data for 1993–2009 and data from coastal and island sea level measurements for 1880–2009, and they obtained 3.2 ± 0.4 mm/yr from the satellite data and 2.8 ± 0.8 mm/yr from the in situ data as the rates of global average sea level changes after correcting for the GIA effects. *Gehrels* [2010, Figure 4] indicates similar magnitude in the present-day global sea level change. We estimate the trend in ocean loading from global sea level rise in a similar way to the computation of the OTL effects. For this, we assumed that the oceans are globally rising with a rate of 3 mm/yr. Although the magnitude depends on the geographical conditions of site, the effects are estimated to be within the ranges of 0.08 to 0.11 mm/yr and −0.11 to −0.12 μGal/yr. If we subtract 0.11 mm/yr and −0.12 μGal/yr from the rates shown in Table 9, we obtain ratios of −0.198 ± 0.088 μGal/mm and −0.183 ± 0.053 μGal/mm for the cases using the PDIMC models of UAF05 and UAF07, respectively.

[46] On the other hand, *Tamisiea* [2011] studied ongoing glacial isostatic contributions to the observations of sea level, and they find that GIA produces a small systematic contribution to the altimetry estimations with a maximum range of −0.15 to −0.5 mm/yr, which is similar in magnitude to that obtained by *Peltier* [2009]. *Bromirski et al.* [2011], who studied the relation between the PDO (Pacific Decadal Oscillation) regime related to the ENSO (El Niño–Southern Oscillation) and the sea level change, find that the sea level rise along the Pacific coast of North America (including the SE-AK area) has been dynamically suppressed since 1980. Moreover, the sea level change shown by *Gehrels* [2010, Figure 4] is considered to be mostly a steric one. Therefore, there is a possibility that our estimation of the effects of the sea level change on our observations might be an over estimation.

[47] Last, as described in section 4.5, the GRACE mascon solutions show a good spatial coherency in the phases over the SE-AK area [*Luthcke et al.*, 2008]. On the other hand, as described in section 4.7, it is known that, due to the complex topography in this area, the ocean tides are largely deformed from those based on the satellite data. Similar situation may be considered in the gravity variations in SE-AK observed from the satellite gravimetry. Therefore, it is important to validate the amplitude of the satellite data with the observations on the ground. In order to obtain a better correction value for the seasonal change to the AG and GPS observations, it should give us useful data to carry out a collocated observation with the AG meter and GPS in SE-AK at a frequency of once every 10 days or once every month over one year, for instance. This kind of data should also provide

useful information to increase the accuracy of the discussion of the GIA effects and of the viscous ratio.

5. Summary

[48] The comparisons between the observations and the model computations indicate that both the gravity and uplift rates obtained from the model predictions are consistent with the observed rates at most sites compared here. Although there are several remaining problems in our model estimations, we can say that, at least, results of the comparison of the observed viscous ratios with model predictions indicate that the observations detect an early stage of the viscoelastic relaxation mainly due to the effects of the post-LIA unloading. Our results also suggest that the viscous ratios depend on the regional history of wastage of glaciers and the ice fields. It may be a point to be noted when applying a method proposed by *Wahr et al.* [1995] to separate the effects of past and present unloading in geodetic observations.

[49] Most of the AG and GPS data used here were obtained from observations made in campaign style and all carried out during the summer season. The agreement between the observations and model predictions indicates that seasonal effects of the hydrology and the cryo-sphere, while substantial, have been minimized by our observational strategy and we consider that the uncorrected effects do not so seriously affect that we must change our conclusions. Of course, improving the estimation of seasonal and inter-annual effects is important and it is desired in order to reduce a possible ambiguity in our discussions. It is also a key to constrain possible lateral variations in the viscoelastic structure beneath SE-AK from the GPS and gravity observations.

[50] Gravity data obtained from satellite missions such as GRACE and GOCE and the data for ice changes observed from SAR technique will greatly improve the accuracy of the estimations of the seasonal and intramural effects due to the changes in the hydrology and cryo-sphere. For the model computation, it is needed to examine our results by comparing with the computations took into account the Earth's compressibility and the degree 1 deformation. These remain for the further studies.

References

Ali, S. T., and A. M. Freed (2010), Contemporary deformation and stressing rates in Southern Alaska, *Geophys. J. Int.*, *183*, 557–571, doi:10.1111/j.1365-246X.2010.04784.x.

Arendt, A. A., K. A. Echelmeyer, W. D. Harrison, C. S. Lingle, and V. B. Valentine (2002), Rapid wastage of Alaska glaciers and their contribution to rising sea level, *Science*, *297*, 382–386, doi:10.1126/science.1072497.

Argus, D. F., R. G. Gordon, M. B. Heflin, C. Ma, R. J. Eanes, P. Willis, W. R. Peltier, and S. E. Owen (2010), The angular velocities of the plates and the velocity of Earth's centre from space geodesy, *Geophys. J. Int.*, *181*, 1–48, doi:10.1111/j.1365-246X.2009.04463.x.

Bilham, R., and G. S. Sasagawa (1994), US geoscience community gains an absolute gravimeter, *Eos Trans. AGU*, *75*(49), 569–570, doi:10.1029/94EO02042.

Boehm, J., A. Niell, P. Tregoning, and H. Schuh (2006), Global Mapping Function (GMF): A new empirical mapping function based on numerical

weather model data, *Geophys. Res. Lett.*, *33*, L07304, doi:10.1029/2005GL025546.

Bromirski, P. D., A. J. Miller, R. E. Flick, and G. Auad (2011), Dynamical suppression of sea level rise along the Pacific coast of North America: Indications for imminent acceleration, *J. Geophys. Res.*, *116*, C07005, doi:10.1029/2010JC006759.

Church, J. A., and N. J. White (2011), Sea-level rise from the late 19th to the early 21st century, *Surv. Geophys.*, *32*, 585–602, doi:10.1007/s10712-011-9119-1.

Dziewonski, A. D., and D. L. Anderson (1981), Preliminary reference earth model, *Phys. Earth Planet. Inter.*, *25*, 297–356, doi:10.1016/0031-9201(81)90046-7.

Elliott, J., C. F. Larsen, J. T. Freymueller, and R. J. Motyka (2010), Tectonic block motion and glacial isostatic adjustment in southeast Alaska and adjacent Canada constrained by GPS measurements, *J. Geophys. Res.*, *115*, B09407, doi:10.1029/2009JB007139.

Fang, M., and B. Hager (2001), Vertical deformation and absolute gravity, *Geophys. J. Int.*, *146*, 539–548, doi:10.1046/j.0956-540x.2001.01483.x.

Farrell, W. E. (1972), Deformation of the Earth by surface loads, *Rev. Geophys.*, *10*, 761–797, doi:10.1029/RG010i003p00761.

Fu, Y., J. T. Freymueller, and T. van Dam (2011), The effect of using inconsistent ocean tidal loading models on GPS coordinate solutions, *J. Geod.*, doi:10.1007/s00190-011-0528-1, in press.

Gehrels, R. (2010), Sea-level changes since the Last Glacial Maximum: An appraisal of the IPCC Fourth Assessment Report, *J. Quat. Sci.*, *25*, 26–38, doi:10.1002/jqs.1273.

Inazu, D., T. Sato, S. Miura, Y. Ohta, K. Nakamura, H. Fujimoto, C. F. Larsen, and T. Higuchi (2009), Accurate ocean tide modeling in southeast Alaska and large tidal dissipation around Glacier Bay, *J. Oceanogr.*, *65*, 335–347, doi:10.1007/s10872-009-0031-y.

James, T. H., and E. R. Ivins (1998), Predictions of Antarctic crustal motions driven by present-day ice sheet evolution and by isostatic memory of the Last Glacial Maximum, *J. Geophys. Res.*, *103*, 4993–5017, doi:10.1029/97JB03539.

Lambert, A., N. Courtier, and T. S. James (2006), Long-term monitoring by absolute gravimetry: Tides to postglacial rebound, *J. Geodyn.*, *41*, 307–317, doi:10.1016/j.jog.2005.08.032.

Larsen, C. F., R. J. Motyka, J. T. Freymueller, K. A. Echelmeyer, and E. R. Ivins (2004), Rapid uplift of southern Alaska caused by recent ice loss, *Geophys. J. Int.*, *158*, 1118–1133, doi:10.1111/j.1365-246X.2004.02356.x.

Larsen, C. F., R. J. Motyka, J. T. Freymuller, K. A. Echelmeyer, and E. R. Ivins (2005), Rapid viscoelastic uplift southern Alaska caused by post-Little Ice Age glacial retreat, *Earth Planet. Sci. Lett.*, *237*, 548–560, doi:10.1016/j.epsl.2005.06.032.

Larsen, C. F., R. J. Motyka, A. A. Arendt, K. A. Echelmeyer, and P. E. Geissler (2007), Glacier changes in southeast Alaska and northwest British Columbia and contribution to sea level rise, *J. Geophys. Res.*, *112*, F01007, doi:10.1029/2006JF000586.

Larsen, C. F., R. M. Hock, A. A. Arendt, and S. L. Zirnheld (2009), Airborne laser altimetry measurements of glacier wastage in Alaska and NW Canada, *Eos Trans. AGU*, *90*(52), Fall Meet. Suppl., Abstract C23C-0508.

Luthcke, S. B., A. A. Arendt, D. D. Rowlands, J. J. Mccarthy, and C. F. Larsen (2008), Recent glacier mass changes in the Gulf of Alaska region from GRACE mascon solutions, *J. Glaciol.*, *54*(188), 767–777, doi:10.3189/002214308787779933.

Miura, S., T. Sato, H. Fujimoto, S. Wenke, J. T. Freymuller, A. Kaufman, and R. Cross (2007), Geodetic measurements for monitoring rapid crustal uplift in southeast Alaska caused by post-glacial rebound—Outline of the project, paper presented at the 7th International Conference on Global Change: Connection to Arctic, Int. Arct. Res. Cent., Fairbanks, Alaska, 19–20 Feb.

Molnia, B. F. (2008), Glaciers of North America—Glaciers of Alaska, in *Satellite Image Atlas of Glaciers of the World*, edited by S. R. Williams Jr. and J. G. Ferrigno, *U.S. Geol. Surv. Prof. Pap.*, *1386-K*, 128–153.

Peltier, W. R. (1974), The impulse response of a Maxwell Earth, *Rev. Geophys.*, *12*(4), 649–669, doi:10.1029/RG012i004p00649.

Peltier, W. R. (2009), Closure of the budget of global sea level rise over the GRACE era: The importance and magnitudes of the required corrections

for global glacial isostatic adjustment, *Quat. Sci. Rev.*, *28*, 1658–1674, doi:10.1016/j.quascirev.2009.04.004.

Sasagawa, G. S., and M. A. Zumberge (1997), Absolute gravity measurements and instrument comparisons in California, paper presented at Chapman Conference, AGU, St. Augustine, Fla.

Sasagawa, G. S., M. A. Zumberge, J. M. Stevenson, T. Lautzenhiser, J. Wirtz, and M. E. Ander (1989), The 1987 Southeastern Alaska gravity calibration range: Absolute and relative gravity measurements, *J. Geophys. Res.*, *94*(B6), 7661–7666, doi:10.1029/JB094iB06p07661.

Sato, T., and H. Hanada (1984), A program for the computation of oceanic tidal loading effects 'GOTIC,' *Publ. Inter. Lat. Obs. Mizusawa*, *18*(1), 29–47.

Sato, T., J. Okuno, J. Hinderer, D. S. MacMillan, H.-P. Plag, O. Francis, R. Falk, and Y. Fukuda (2006), A geophysical interpretation of the secular displacement and gravity rates observed at Ny-Ålesund, Svalbard in the Arctic—Effects of post-glacial rebound and present-day ice melting, *Geophys. J. Int.*, *165*, 729–743, doi:10.1111/j.1365-246X.2006.02992.x.

Sato, T., S. Miura, Y. Ohta, H. Fujimoto, W. Sun, C. F. Larsen, M. Heavner, A. M. Kaufman, and J. T. Freymueller (2008), Earth tides observed by gravity and GPS in southeastern Alaska, *J. Geodyn.*, *46*, 78–89, doi:10.1016/j.jog.2008.03.004.

Sato, T., C. F. Larsen, S. Miura, Y. Ohta, H. Fujimoto, W. Sun, R. J. Motyka, and J. T. Freymuller (2011), Reevaluation of the viscoelastic and elastic responses to the past and resent-day ice changes in Southeast Alaska, *Tectonophysics*, *511*, 79–88, doi:10.1016/j.tecto.2010.05.009.

Sella, G. F., S. Stein, T. H. Dixon, M. J. Craymer, T. S. James, S. Mazzotti, and R. K. Dokka (2007), Observation of glacial isostatic adjustment in "stable" North America with GPS, *Geophys. Res. Lett.*, *34*, L02306, doi:10.1029/2006GL027081.

Spada, G. (2003), *The Theory Behind TABOO*, Samizdat, Golden, Colo.

Spada, G., et al. (2003), *TABOO User Guide*, Samizdat, Golden, Colo.

Spada, G., et al. (2004), Geodesy: Modeling Earth's post-glacial rebound, *Eos Trans. AGU*, *85*(6), 62–64, doi:10.1029/2004EO060007.

Spada, G., V. R. Barletta, V. Klemann, R. E. M. Riva, Z. Martinec, P. Gasperini, B. Lund, D. Wolf, L. L. A. Vermeersen, and M. A. King (2011), A benchmark study for glacial isostatic adjustment codes, *Geophys. J. Int.*, *185*, 106–132, doi:10.1111/j.1365-246X.2011.04952.x.

Suito, H., and J. T. Freymueller (2009), A viscoelastic and afterslip postseismic deformation model for the 1964 Alaska earthquake, *J. Geophys. Res.*, *114*, B11404, doi:10.1029/2008JB005954.

Sun, W., S. Miura, T. Sato, T. Sugano, J. T. Freymueller, M. Kaufman, C. F. Larsen, R. Cross, and D. Inazu (2010), Gravity measurements in southeastern Alaska reveal negative gravity rate of change caused by glacial isostatic adjustment, *J. Geophys. Res.*, *115*, B12406, doi:10.1029/2009JB007194.

Tamisiea, M. E. (2011), Ongoing glacial isostatic contributions to observations of sea level change, *Geophys. J. Int.*, *186*, 1036–1044, doi:10.1111/j.1365-246X.2011.05116.x.

Tanaka, Y., V. Klemann, and J. Okuno (2009), Application of a numerical inverse Laplace integration method to surface loading on a viscoelastic compressible Earth model, *Pure Appl. Geophys.*, *166*, 1199–1216, doi:10.1007/s00024-009-0508-y.

Tushingham, A. M., and W. R. Peltier (1991), ICE-3G: A new global model of late Pleistocene deglaciation based upon geophysical predictions of post-glacial relative sea level change, *J. Geophys. Res.*, *96*, 4497–4523, doi:10.1029/90JB01583.

Wahr, J., H. DaZhong, and A. Trupin (1995), Predictions of vertical uplift caused by changing polar ice volumes on a viscoelastic Earth, *Geophys. Res. Lett.*, *22*(8), 977–980, doi:10.1029/94GL02840.

J. T. Freymueller, C. F. Larsen, and R. J. Motyka, Geophysical Institute, University of Alaska Fairbanks, Fairbanks, AK 99801, USA.

H. Fujimoto, D. Inazu, S. Miura, Y. Ohta, and T. Sato, Research Center for Prediction of Earthquakes and Volcanic Eruptions, Tohoku University, Sendai 980-8578, Japan. (tsato@aob.gp.tohoku.ac.jp)

T. Sugano, Earthquake Research Institute, University of Tokyo, Tokyo 113-0032, Japan.

W. Sun, Key Laboratory of Computing Geodynamics, Graduate University of Chinese Academy of Science, Beijing 100049, China.